JOURNAL OF PROPULSION AND POWER
Vol. 23, No. 2, March–April 2007

Optimal Classification Criterions of Hypersonic Inlet Start/Unstart

Daren Yu,* Juntao Chang,† Wen Bao,‡ and Zongxia Xie§
Harbin Institute of Technology, 150001 Heilongjiang, People's Republic of China

DOI: 10.2514/1.24640

Inlet start/unstart detection is one of the most important issues of hypersonic inlet and is also the foundation of protection control of a scramjet. To solve this problem, the 2-D inner steady flow of a hypersonic inlet was numerically simulated in different freestream conditions and backpressures with a Reynolds-averaged Navier–Stokes solver using a renormalization group *k–e* turbulence model; two different inlet unstart phenomena were analyzed. The feature selection of the pattern classification of hypersonic inlet start/unstart was performed based on "numerical experimental" data by the support vector machine-recursive feature elimination algorithm. The optimal classification criterions of inlet start/unstart were obtained with the Fisher linear discriminant analysis by maximizing the between-class distance of the inlet/unstart sample set and minimizing the within-class, and the physical significance of the classification criterions was explained. The idea of classification criterions used in the Central Institute of Aviation Motors/NASA flight test and possible reasons why the control system could not properly sense inlet start/unstart were discussed. In conclusion, it is useful to introduce the support vector machine-recursive feature elimination algorithms and the Fisher linear discriminant analysis to acquire the optimal classification criterions of inlet start/unstart.

Nomenclature

M_∞	=	Mach number of the freestream
p	=	pressure transformed from p_1 and p_2
p_{back}	=	pressure at the exit of isolator
$p_{\max}$	=	pressure larger than the maximal sustainable backpressure of the isolator
$p_{\min}$	=	mass-weighted average pressure at the entrance of isolator
p_s	=	surface pressure of the inlet
p_1	=	pressure at x_1, pressure behind the first oblique shock
p_2	=	pressure at x_2, pressure under the lip
p_3	=	pressure at x_3, pressure near the entrance of isolator
p_∞	=	pressure of the freestream
T_∞	=	static temperature of the freestream
x	=	axis location of the inlet
x_1	=	shown in Fig. 1
x_2	=	shown in Fig. 1
x_3	=	shown in Fig. 1
α	=	angle of attack of the freestream

I. Introduction

THE performance of a ramjet–scramjet powered hypersonic vehicle is determined by its inlet efficiency. Specifically, the inlet wave system influences compression efficiency, mass capture, and combustion stability. The unstart phenomenon is one of the most important issues of the hypersonic inlet. The disturbances which can induce inlet unstart can be either the variation of flight conditions (i.e., angle of attack, freestream Mach number, freestream pressure, etc.) or the disturbance of the combustor. For hypersonic airbreathing engines, inlet unstart causes a large drop of both engine thrust and specific impulse, thus it may cause catastrophic damage during hypersonic flight. The determination of inlet start/unstart is an important aspect in the ground and flight test, without which performance and operational envelopes cannot be properly determined. Furthermore, from the viewpoint of the engine control systems, disturbances are introduced into the engine control system by accelerations that are several times larger than those of a transport. Quick inlet start/unstart detection is required because the loss of engine thrust caused by inlet unstart results in a deceleration of the space plane or even a mission failure [1,2].

Unstart phenomena of the hypersonic inlet have been very active fields of research in the last decades, and there have been many papers devoted to this subject [3–14]. Generally speaking, there are two approaches to the inlet unstart. The first one is based on numerical simulation. With current powerful computers, CFD (computational fluid dynamics) can be used as a preliminary tool to analyze the phenomena and mechanism of the inlet unstart. Mayer and Paynter [3,4] used an Euler solver and simulated an axisymmetric inlet unstart due to the variation of freestream variables such as temperature, velocity, and pressure. Neaves and McRae [5] developed a dynamic solution-adaptive grid algorithm introduced by Benson and McRae [6] and simulated the 3-D inlet unstart caused by a combustor perturbation. Zha [7,8] investigated an unstart transient mechanism of a typical axisymmetric HSCT (high speed civil transport) inlet at angle of attack using CFD. Cox [9] presented several mechanisms of hypersonic inlet unstart, including backpressure unstart, overcontraction unstart, and angle of attack unstart. The second approach is based on experimental investigation. Schmitz [10] and Van Wie [11] analyzed the major factors that influence the inlet operation mode and studied the start/unstart characteristic of 2-D hypersonic inlet. Reinartz [12] and Emami [13] studied the variation of isolator geometry and its influence on the overall inlet compression efficiency; the investigation shows that the sustainable backpressure is strongly influenced by the isolator length.

However, few numerical and experimental investigations have been reported on the detection of hypersonic inlet start/unstart. The detection [14] has been proposed and several measurement techniques provided useful information by which to evaluate the inlet operating mode that are the flow visualization technique using the

Received 16 April 2006; revision received 1 August 2006; accepted for publication 13 August 2006.

*Professor, School of Energy Science and Engineering; yudaren@hcms.hit.edu.cn.

†Ph.D. Candidate, School of Energy Science and Engineering; juntao_chang@yahoo.com.cn.

‡Professor, School of Energy Science and Engineering; baowen@hcms.hit.edu.cn.

§Ph.D. Candidate, School of Energy Science and Engineering; xiezongxia@hcms.hit.edu.cn.

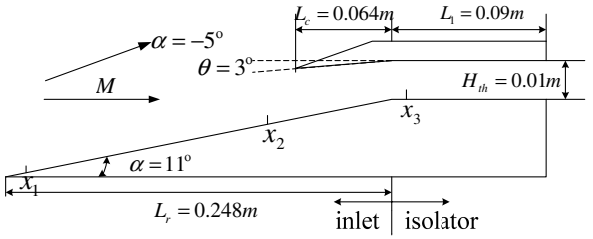

Fig. 1 Geometric sketch of inlet model.

shadowgraph/schlieren windows, the rapid change of steady pressure just upstream and downstream of the inlet throat, and the dynamic pressure amplitude time history near the inlet throat. The visualization technique is complex and not practical to the flight test; the other two are validated using the test data at only zero angle of attack. In the CIAM/NASA (Central Institute of Aviation Motors) flight test [15], the engine control system determines the inlet start/unstart by a ratio of the pressure near the entrance of the isolator to the pressure under the lip. Unfortunately, the inlet operation mode is not properly sensed, which results in the part failure of the flight test.

Learning pattern classification has been developed in the past decades [16]. Pattern classification is the act of taking in the raw data and taking an action based on the "category" of the pattern. The objects to be classified are first sensed by a transducer (camera), whose signals are preprocessed, then the features extracted, and finally the classification emitted. This is the common procedure of pattern classification. In this paper, the study is focused on the method of pattern classification of hypersonic inlet start/unstart based on the simulation results. To establish the classification criterions, the inlet unstart phenomena (backpressure unstart, low Mach number unstart) were studied at first step. Based on the "numerical experiment" data, the SVM-RFE (support vector machine-recursive feature elimination) algorithms by which the feature selection is performed and FLD (Fisher linear discriminant) analysis by which the optimal classification hyperplane is obtained are introduced to solve the pattern classification of hypersonic inlet start/unstart. The rest of this paper is organized as follows. Section II states data preparation for pattern classification of hypersonic inlet start/unstart. Section III presents the feature selection of inlet start/unstart by the SVM-RFE algorithm. The optimal classification criterions and analysis are given in Sec. IV. Section V presents some conclusions.

II. Data Preparation for Pattern Classification of Hypersonic Inlet Start/Unstart

Pattern classification is the act of taking in the raw data and taking an action based on the category of the pattern. For the pattern classification of hypersonic inlet start/unstart, the first step is to obtain the surface pressure distributions which include the inlet start and inlet unstart. The data can be acquired by the numerical simulation or experiment to the hypersonic inlet.

A. Inlet Model and Numerical Method

The overall inlet geometry is based on the similar inlet model tested within the frame of earlier Langley Research Center activities [13]. The two-dimensional inlet model was designed at a 2% scale to replicate the generic feature of a hypersonic propulsion system. The inlet model mentioned above is simplified in computation because the principal aim of this paper is to research the pattern classification of inlet start/unstart. The computational model includes an inlet and constant area isolator only. Figure 1 shows the geometric sketch of the inlet model.

The computation is performed using the finite-volume technique with upwind discretization to solve the three-dimensional compressible Reynolds-averaged Navier–Stokes equations. The air is considered to be a calorically perfect gas with constant ratio of specific heat, $r = 1.4$. The space discretization is performed by a cell-centered formulation. A renormalization group k–e turbulence model is implemented for turbulent flows. The near-wall treatment adopts nonequilibrium wall functions which are recommended for use in complex flows involving separation, reattachment, and impingement where the mean flow and turbulence are subjected to severe pressure gradients and change rapidly. The supersonic inflow is defined by specifying the boundary conditions given in Table 1, where the definition of α is referred to Fig. 1. In the case of predominant supersonic outflow, the variables are completely extrapolated from the interior to the boundary. Otherwise, the influence of the throttle is simulated with a prescribed backpressure P_{back} at the outflow boundary, and the remaining variables are extrapolated. At solid walls, the no-slip boundary condition is enforced by setting the velocity components to zero. The adiabatic energy boundary condition is directly applied by zeroing the contributions of the wall faces to the dissipative fluxes.

Table 1 Boundary conditions for cases I, II, and III

Case	M_∞	T_∞, K	P_∞, Pa	P_{back}, Pa	Angle of attack α, deg
I	4	216.6	8471	$[p_{\min}, p_{\max}]$	−10, −5, 0, 5, 10
II	5	216.7	5415	$[p_{\min}, p_{\max}]$	−10, −5, 0, 5, 10
III	6	219.1	3743	$[p_{\min}, p_{\max}]$	−10, −5, 0, 5, 10

B. Numerical Accuracy Analysis

To ensure convergence of the numerical solution, the residual ($L2$ norm) is monitored in Fig. 2. The solution can be considered as converged after approximately 6000 iterations. At this stage, the continuity residual, x-velocity residual, and energy residual reach their minimum values after falling for over 4 orders of magnitude. The turbulence residual has a 6 orders of magnitude decrease. An additional convergence criterion enforced in this current analysis requires the difference between computed inflow and outflow mass flux to drop below 0.5%. The evaluation was performed using the coarse mesh.

The performance of a grid sensitivity analysis confirmed that the grid resolution used here is sufficient to capture the physically relevant features. In Fig. 3, the static pressure distributions along the cowl and the ramp surfaces are shown for three different grid-refinement levels: coarse (321×30), medium (642×50), and fine (1158×70); the maximum discrepancy between the three mesh levels is less than 3%. The calculations were performed on a workstation. The CPU time needed for computation is about 1 h for the coarse mesh, 4 h for the medium mesh, and 10 h for the fine mesh. Out of this analysis, the medium grid was selected, and all results shown are computed applying this resolution. The use of a medium grid resolution greatly saves the CPU time. To ensure the accuracy of the turbulence flow solution, a value of y^+ below 1 is realized for the main portion of the wall flow region. To simulate the interaction between the shock and the boundary layer, the intersection, and the reflection of the wave system, calculate the flowfield at first, and perform the mesh self-adaptation technology based on the pressure gradient and continue to compute.

The accuracy of the current numerical investigation is evaluated by comparison with the experimental results. The experimental data

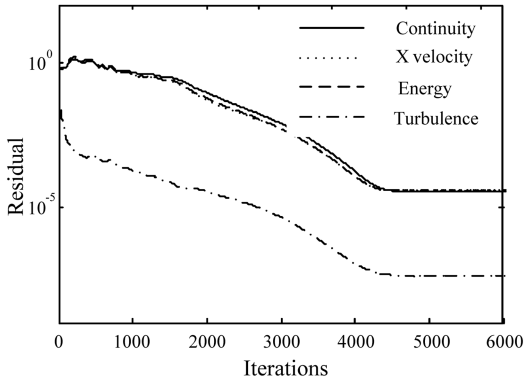

Fig. 2 Residuals for supersonic inlet computation.

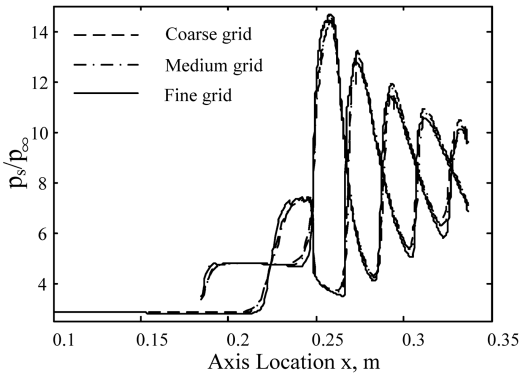

Fig. 3 Surface pressure distributions for refined grid.

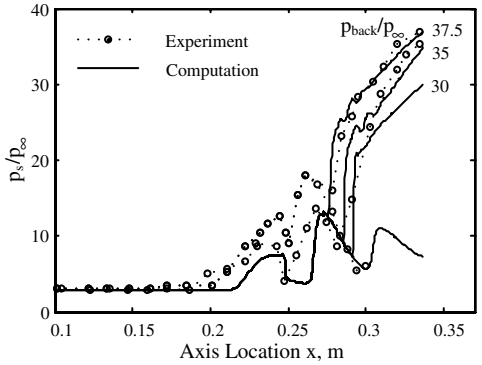

Fig. 4 Surface pressure distributions with different backpressures $M_\infty = 4$ and $\alpha = 0$.

are referred to Fig. 7 and Fig. 19(e) in [13]. The surface pressure distributions are shown in Fig. 4, allowing for a qualitative comparison between numerical and experimental results. Here, a discrepancy in the ramp pressure distributions can be seen, but both the overall pressure distributions are consistent, and the maximal pressure ratios before inlet unstart are both 37.5. The reason for the discrepancy is probably the deficiency of the turbulence model, the differences between experiment and computation conditions, or the measurement error of the sensor. In a word, the computation results of hypersonic inlet accord with the physical conception of the aerodynamics. It can reveal the intersection of oblique shock wave and expansion wave and capture the primary characteristic of internal flowfield. The simulation results can be used as data to investigate the pattern classification of hypersonic inlet start/unstart.

C. Inlet Unstart Data Composition and Analysis

The inlet unstart probably occurs at the range Mach 2 to Mach 12; it is most likely at the low Mach number. The risk to the vehicle increases as velocity increases. The inlet unstart at higher Mach number might be too much overpressure for the inlet structure to handle without larger vehicle weight penalties. At lower Mach number, the vehicle might be catastrophically uncontrollable after inlet unstart, even if the structure could handle inlet unstart overpressures. There are two main classes of inlet unstart for the fixed-geometry hypersonic inlet, one is backpressure unstart, and the other is low Mach number unstart. The unstart data set includes the two classes of inlet surface pressure distributions.

In scramjet, a precombustion shock system is developed inside of the isolator because of the subsequent high-pressure combustion zone. To produce a similar shock wave system in the test, the effect of the operating engine is simulated by a specified backpressure. Figure 4 shows surface pressure distributions with different backpressure ratios. The high backpressure leads to the separation of the boundary layer. The pressure buildup proceeds continuously due to the rapidly growing boundary layer. As the backpressure increases, the onset of pressure buildup moves upstream into the

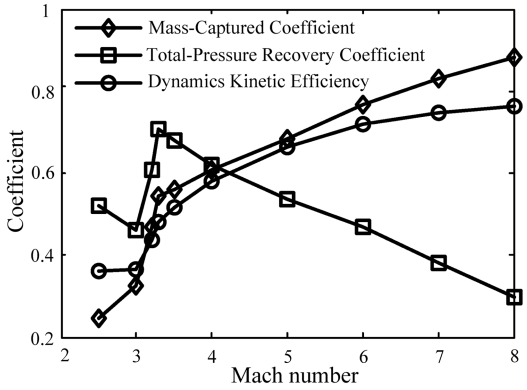

Fig. 5 Variations of mass-captured coefficient, total-pressure recovery coefficient, and dynamics kinetic efficiency with the Mach number of freestream.

isolator. At $p_{back}/p_\infty = 37.5$, the complete isolator contributes to the pressure buildup, and the maximum pressure ratio p_{back}/p_∞ is achieved. After even a slight shift of the operating point ($p_{back}/p_\infty = 37.5$), the pressure rise is pushed forward into the contracting part of the inlet. A further increase of the backpressure causes a severe flow blockage and results in a strong decrease of captured mass flow. In this condition, the inlet flowfield is unstable and the inlet is no longer started.

The internal contraction ration of the hypersonic inlet is about 1.9, which is above the Kantrowitz limit for self-starting. Figure 5 shows the variations of the mass-captured coefficient, the total-pressure recovery coefficient, and the kinetic energy efficiency with the Mach number of freestream. As the Mach number of freestream decreases, the mass-captured coefficient and kinetic energy efficiency gradually decrease and the total-pressure recovery coefficient increases. When Mach number decreases to Mach 3.2, the performance parameter varies abruptly because the separated flow appears and the backward shock is formed; thus the inlet is no longer started. The starting Mach number of the hypersonic inlet is about 3.2 at the attack of angle zero. There probably exist two stable solutions at the same boundary conditions; at this condition the solutions depend on the initial values of the hypersonic inlet. If the initial values of the inlet are started, the inlet is started or otherwise unstarted. The data set includes the two solutions of the hypersonic inlet at the same boundary conditions. Here the term "started" is used to denote the operation mode under which the shock system structures in the internal portions of the inlet do not alter the mass-captured characteristics. This is the essence difference between inlet start and unstart. However you approach the CFD solutions, the inlet start or unstart can be defined based on the mass-captured characteristics.

III. Feature Selection of Inlet Start/Unstart Classification Based on SVM-RFE

Generally speaking, for the fixed-geometry inlet, the boundary between the inlet start and unstart is a very complex function of the Mach number of freestream, angle of attack, pressure of freestream, and the pressure at the exit of the isolator (or fueling rate). Determining the boundary approximate function expression is difficult involving these variables with uncertainty. So the pattern classification of hypersonic inlet start/unstart is difficult.

The three sets of conditions identified in Table 1 were analyzed as representative operating conditions for a hypersonic inlet. The ramp surface pressure distributions of the inlet at different boundary conditions are shown in Fig. 6. It includes 117 different surface pressure distributions of inlet started and 62 distributions of inlet unstarted. The high dimension of the data set offers great difficulty in understanding the data, constructing classifier for pattern classification, and machine learning. As can be seen from Fig. 6, there are no intuitively distinct features by which the inlet start/unstart could be classified. Therefore, it is necessary to introduce the knowledge of the feature selection and various intelligence algorithms to solve classification problems of inlet start/unstart. The

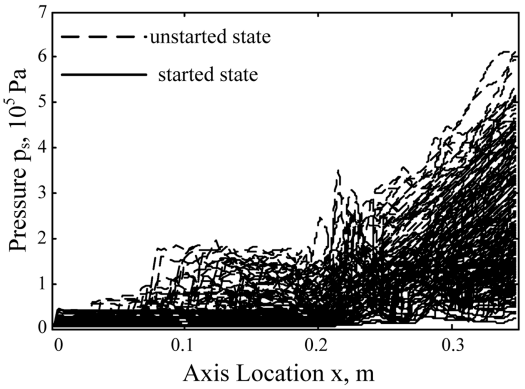

Fig. 6 Surface pressure distributions with different boundary conditions.

aim of the feature selection is to find a subset of original features from a given dataset by removing irrelevant and redundant features [17]. In recent years the feature selection has attracted much attention from a pattern recognition and machine learning society [18–20]. Feature selection can provide a faster and more cost-effective predictor and improve the prediction performance [21].

There are many statistical methods of clustering and classification used for feature selection. SVM proposed in the 1990s by Vapnik has already been known as an efficient tool for discovering informative feature attributes [22]. A lot of researches on SVM and using SVM were carried on. In 2002, SVM was first applied to gene selection for cancer classification as a method of feature selection; it is called SVM-RFE [23]. In 2003, Rakotomamonjy [24] studied variable selection using different kinds of SVM-based criteria, such as weight vector, the radius/margin bound, and so on. However, the methods above are just used for binary-class classification problems. Li [25] et al. have studied the feature selection for multiclass classification using SVM in 2004. In 2005, Duan [26] et al. extended the SVM-RFE method to multiclass problems by computing the feature ranking score from a statistical analysis of weight vectors of multiple linear SVM trained on subsamples of the original training data. SVM-RFE is an application of RFE using SVM criteria for ranking. RFE is a method which performs backward feature elimination, starting with all features and then removing some irrelevant features according to a ranking criterion until satisfaction with a stop criterion is achieved. The stop criterion is to find m features which results in the largest boundary of class separation or the experience risk begins to go down [27].

Consider the following two-category classification problem: $(x_1, y_1), (x_2, y_2), \ldots, (x_i, y_i), \ldots, (x_l, y_l),\ x_i \in R^n,\ y_i \in \{-1, +1\}$; here x_i is a training example and y_i is the corresponding class. The decision function could be obtained by maximizing the distance between the two classes, $f(x) = \mathrm{sgn}(w \cdot x - b) = \mathrm{sgn}[\sum_{\mathrm{SVs}} y_i a_i (x_i \cdot x) - b]$. Here a is the Lagrange multiplier vector, $w = \sum_{\mathrm{SVs}} y_i a_i x_i$ is the weight magnitude, and w^2 is a measure of predictive ability which is inversely proportionate to the margin.

The main iterative procedures are given as follows:

1) Train SVM and get the original experience risk and the weight of every feature $w_{(t)} = \sum_{\mathrm{SVs}} y_i a_i x_{i(t)}$; here $x_{i(t)}$ is the value of the tth feature of the ith sample.

2) Rank the features by the values of w^2.

3) Remove the feature with the smallest value w^2, retrain the SVM with the reduced set of features, and get the new experience risk and the weight of every feature.

4) If the new experience risk is equal to or larger than the original one, go to step 2) or else break.

5) The subset is what we want ultimately.

The total sample set includes 117 surface pressure distributions of the inlet started, 62 distributions of the inlet unstarted which contain two classes of inlet unstart phenomena, and every pressure distribution includes 642 data. The dimension of the total sample set is 642×179. The feature selection is studied based on the train sample set by using the algorithm of SVM. First of all, use all the feature attributions to train SVM and get their accuracies. Then apply SVM-RFE to select the relevant feature subset. Finally the two classes of feature attributions [3, 7, 11] and [80, 91, 99, 110, 122, 130] are found; here 3 denotes the third pressure point for every surface pressure distribution and so on. The axis location of every feature attribution is as follows: 3: 0.0039 m, 7: 0.0117 m, 11: 0.0200 m, 80: 0.1546 m, 91: 0.1761 m, 99: 0.1851 m, 110: 0.1884 m, 122: 0.1919 m, and 130: 0.1942 m. Three groups of 18 combinations are achieved based on the two classes of feature attributions and are shown in Table 2.

There are three groups of 18 different combinations which can be chosen for the pattern classifications of hypersonic inlet start/unstart. Here the 1-1 combination of [3, 80] is chosen as an example to illustrate the pattern classification of inlet start/unstart. First select 70% of the samples as the train set random. The classification hyperplane $p_2 - 1.0033p_1 - 6995.3 = 0$ is obtained, and here p_1 and p_2 are the pressure of 3rd and the 80th, respectively. There exist two boundaries, one is the boundary of start, and the other is the boundary of unstart. The classification criterions are described as follows. If $p_2 - 1.0033p_1 - 14301 > 0$, the inlet is unstarted; if $p_2 - 1.0033p_1 + 310.4 < 0$, the inlet is started. The classification hyperplane is validated by the remnant 30% of samples, which is shown in Fig. 7a. Secondly select 70% of the samples as the train set random. The classification hyperplane can be obtained by using the same method, and it is validated by the remnant 30% of samples shown in Fig. 7b.

There exists a combination of feature attributions which has the maximal between-class scatter distance and minimum within-class scatter distance. The FLD analysis is introduced to find the combination by which the optimal classification criterions of inlet start/unstart are obtained.

IV. Optimal Classification Criterions of Inlet Start/Unstart Based on FLD Analysis

The FLD analysis has been widely used in pattern classification. Fisher [28] proposed this approach for taxonomic classification at first. Cui et al. [29] employed a similar algorithm (they called it the most discriminating feature—MDF) for hand sign recognition. Liu [30] adopted FLD to extract the algebraic features of handwritten characters. Belhumeur et al. [31] use FLD to develop a very efficient approach for face recognition. The details of FLD analysis are discussed in the next section.

A. FLD Analysis

The FLD analysis [28] is the benchmark for the linear discrimination between two classes in multidimensional space. It is extremely quick to calculate because it is based on the first and second moments of each distribution only. It may be also shown to maximize a measure of the separation which is not specific to a particular distribution type.

Table 2 Different combinations of feature attributions

Group one, sequence no.	1-1	1-2	1-3	1-4	1-5	1-6
Feature attributions	[3, 80]	[3, 91]	[3, 99]	[3, 110]	[3, 122]	[3, 130
Group two, sequence no.	2-1	2-2	2-3	2-4	2-5	2-6
Feature attributions	[7, 80]	[7, 91]	[7, 99]	[7, 110]	[7, 122]	[7, 130]
Group three, sequence no.	3-1	3-2	3-3	3-4	3-5	3-6
Feature attributions	[11, 80]	[11, 91]	[11, 99]	[11, 110]	[11, 122]	[11, 130]

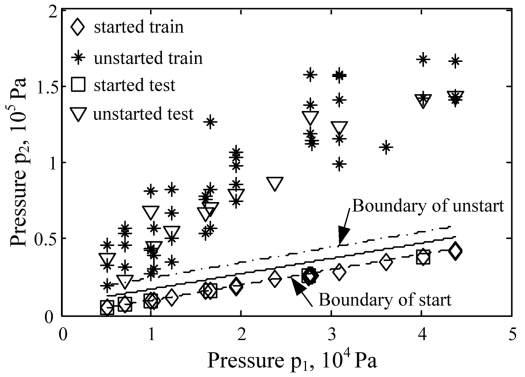

a) Classification and test I

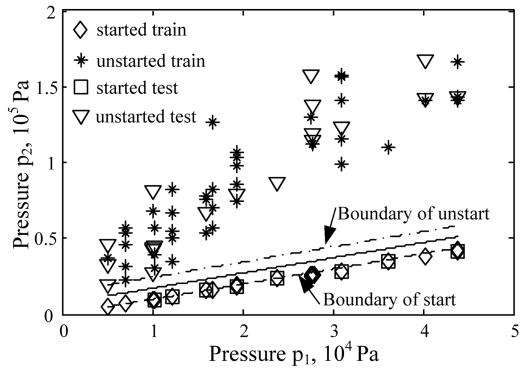

b) Classification and test II

Fig. 7 Classification and test of hypersonic inlet start/unstart.

Suppose that we have a set of n-dimensional samples $x_1, \ldots, x_n$ belonging to c different classes with n_i samples in the subset D_i labeled w_i, $i = 1, \ldots, c$. Then the objective of FLD analysis is to seek the direction w, not only maximizing the between-class scatter matrix of the projected samples, but also minimizing the within-class, such that the following object function $J(w) = w^T S_B w / w^T S_w w$ is maximum. Here S_B and S_w are the between-class scatter matrix and the within-class scatter matrix. $S_B = \sum_{i=1}^{c} N_i(\mu_i - \mu)(\mu_i - \mu)^T$, μ is the sample mean of the whole set, $\mu = \frac{1}{N}\sum_{i=1}^{N} x_i \; i = 1, 2, \ldots, N$, μ_i is the sample mean for the class labeled w_i, $\mu_i = \frac{1}{N_i}\sum_{x \in c_i} x \; i = 1, 2, \ldots, k$. $S_W = \sum_{i=1}^{c} S_i$. Here the scatter matrix S_i, corresponding to the class labeled w_i, is defined as $S_i = \sum_{x \in D_i}(x - \mu_i)(x - \mu_i)^T$, $i = 1, \ldots, c$.

It is easy to know that a vector w that maximizes $J(w)$ must satisfy $S_B w = \lambda S_w w$. If S_W is nonsingular, we can obtain a conventional eigenvalue problem by writing $S_W^{-1} S_B w = \lambda w$. It is obvious that the at most $c - 1$ class of features may be extracted from the above procedures because the rank of S_B is at most $c - 1$.

B. Optimal Classification Criterions of Inlet Start/Unstart

The objective function $J(w)$ is the ratio of the between-class scatter distance to the within-class. The goal is to find the maximum $J(w)$ among the 18 different combinations to maximize the between-class scatter distance and minimize the within-class. The optimal project orientations w and $J(w)$ of every combination are obtained by maximizing $J(w)$. $J(w)$ of different combinations is shown in Table 3. And in Fig. 8, $J(w)$ gradually decreases in three different groups of combinations, respectively; $J(w)$ of combinations 1-1, 2-1, and 3-1 is the maximum of the three different groups, respectively. The combination of 1-1 is chosen to obtain the optimal classification criterions of inlet start/unstart, and the corresponding coordinate transform is $p = p_1 - 0.557 p_2$; here p_1 is the 3rd and p_2 is the 80th pressure point. The classification criterions are described as follows. If $p > 2454 p_a$, the inlet is started; else if $p < -4950 p_a$, the inlet is unstarted. Finally the classification criterions are validated by using another part test sample set, which is shown in Fig. 9. The optimal classification hyperplane of inlet start/unstart using the combinations of 1-1, 2-3, and 3-6 are shown in Figs. 9a–9c. The distance between the boundary of the inlet start and the unstart is 7404 p_a, 5139 p_a, and 4471 p_a, which denotes the robustness of classification criterions.

Table 3 $J(w)$ at different combinations

Sequence no.	1-1	1-2	1-3	1-4	1-5	1-6
$J(w)$	0.0952	0.0734	0.0723	0.0687	0.0643	0.0618
Sequence no.	2-1	2-2	2-3	2-4	2-5	2-6
$J(w)$	0.0940	0.0728	0.0717	0.0681	0.0638	0.0613
Sequence no.	3-1	3-2	3-3	3-4	3-5	3-6
$J(w)$	0.0885	0.0689	0.0678	0.0642	0.0603	0.0581

C. Physical Significance and Analysis of Classification Criterions

As discussed above, the inlet start/unstart can be determined by two pressure points p_1 and p_2. The physical significance of the classification criterions is explained below. p_1 is located behind the first oblique shock, and its magnitude depends on the intensity of shock, namely, depends on M_∞, p_∞, and α. The magnitude of p_1 denotes the freestream conditions. If the freestream conditions are fixed, the inlet start/unstart can be determined by only p_2 for the fixed-geometry inlet. When the inlet is unstart, the separated flow appears and the backward shock is formed, which results in an abrupt and large increase of p_2. However the freestream conditions are variational, and there p_2 of the inlet started at higher Mach number and positive angle of attack is greater than p_2 of inlet unstarted at lower Mach number and negative angle of attack. Thus determining the inlet weather start or unstart by only p_2 is not enough; p_1 which denotes the freestream conditions should be added.

In the CIAM/NASA ground and flight test [15], the scramjet control system determines the inlet start/unstart by the ratio of the pressure near the entrance of the isolator to the pressure under the lip. If the ratio is less than one, the inlet is start, else unstart. The inlet operation mode is not properly sensed, which results in the part failure of the flight test. Now the idea of the inlet start/unstart classification criterions [15] is applied to the inlet in this paper. The classification criterion of this inlet start/unstart is the relationship between p_3 and p_2. Figure 10 shows that for p_3 and p_2 at different freestream conditions (including M_∞, p_∞, and α), the classification hyperplane of inlet start/unstart is not in existence. Figure 11 shows that for p_3 and p_2 at different M_∞, p_∞ and the same $\alpha = 0$, the classification hyperplane of inlet start/unstart could be found obviously. There exists a big difference p_3/p_2 between points 1 and 2 which both denote the inlet start. Point 2 denotes that the backpressure has a strong effect on the inlet flowfield in contrast with 1, which causes more increase of p_3/p_2. So the idea of the classification criterions [15] only fits the same α and this is the possible reason why the control system could not properly sense the inlet start/unstart.

D. Function of the Isolator Belt

The process from the inlet start to inlet unstart is not continuous, but catastrophic. There exists an isolated belt between the boundary

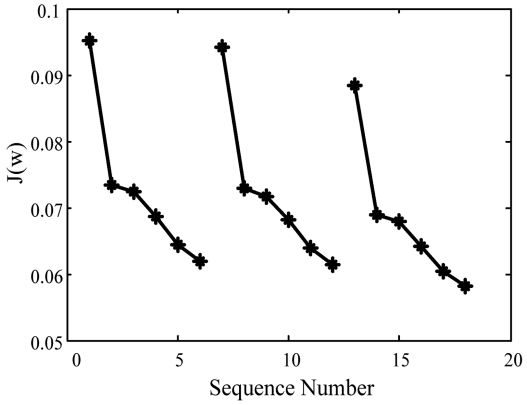

Fig. 8 Variation of $J(w)$ with different combinations.

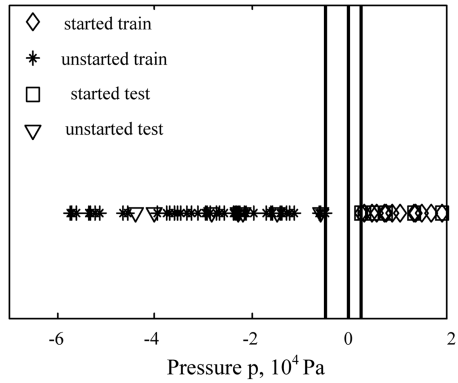

a) Optimal classification hyperplanes of the combination 1-1

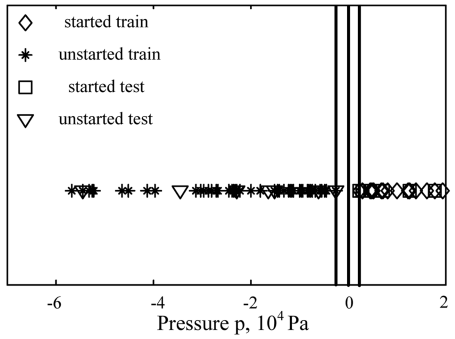

b) Optimal classification hyperplanes of the combination 2-3

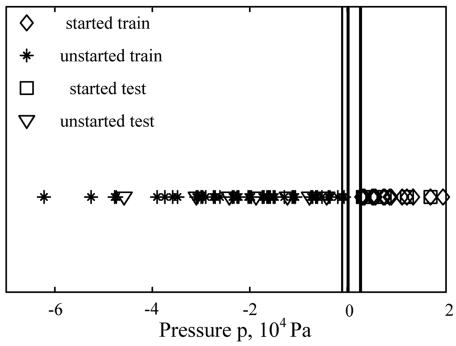

c) Optimal classification hyperplanes of the combination 3-6

Fig. 9 Optimal classification hyperplanes of inlet start/unstart.

of inlet start and unstart, which can be seen in Figs. 7 and 9. In ground and flight test, there probably exist some points from which the inlet start/unstart could not be determined appearing in the isolated belts due to sensor noises, when the decision making of the engine control system is different from the inlet start and unstart. If there exists no isolated belt between the boundary of inlet start and unstart, the pattern classification of inlet start/unstart is easily false due to the

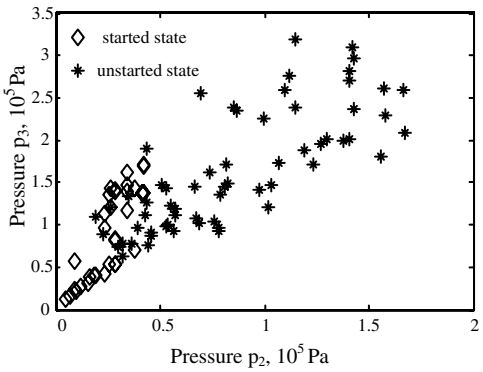

Fig. 10 p_3 and p_2 at different M_∞, p_∞, and α.

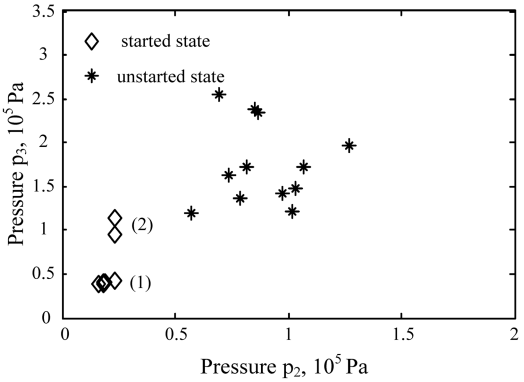

Fig. 11 p_3 and p_2 at different M_∞ and p_∞.

sensor noises. The isolated belt decreases the impact of the measurement noise to the hypersonic inlet start/unstart classification to some extent. The wider the isolated belts, the more robust the classification criterions. The main function of the isolated belts is to improve the reliability of the pattern classification of inlet start/unstart and indicate the inlet unstart in advance; efficient measures can be taken to avoid this catastrophe.

V. Conclusions

The investigation of the pattern classification of hypersonic inlet start/unstart is motivated by the need for the protection control system of scramjets. For this investigation, the SVM-RFE algorithm and FLD analysis methods are introduced to solve the pattern classification of inlet start/unstart in this paper. The algorithm can guarantee the optimization of classification criterions. The classification criterions of the hypersonic inlet start/unstart are given and the validation results prove the validity of the classification criterions. There exists an isolated belt between the boundary of inlet start and unstart. The isolated belt decreases the impact of the measurement noise to the hypersonic inlet start/unstart classification to some extent. The wider the isolated belts, the more robust the classification criterions will be.

References

[1] Campbell, D. H., "F-12 Series Aircraft Propulsion System Performance and Development," *Journal of Aircraft*, Vol. 11, No. 11, 1974, pp. 670–676.

[2] Seddon, J., and Goldsmith, E. L., *Intake Aerodynamics*, AIAA Educational Series, AIAA, Washington, D.C., 1989, pp. 149–168.

[3] Mayer, D., and Paynter, G. C., "Prediction of Supersonic Inlet Unstart Caused by Freestream Disturbances," *AIAA Journal*, Vol. 33, No. 2, 1995, pp. 266–275.

[4] Mayer, D., and Paynter, G. C., "Boundary Conditions for Unsteady Supersonic Inlet Analyses," *AIAA Journal*, Vol. 32, No. 6, 1994, pp. 1200–1206.

[5] Neaves, M. D., McRae, D. S., and Edwards, J. R., "High-Speed Inlet Unstart Calculations Using an Implicit Solution Adaptive Mesh Algorithm," AIAA Paper 2001-0825, Jan. 2001.

[6] Benson, R. A., and McRae, D. S., "Numerical Simulations of the Unstart Phenomenon in Supersonic Inlet/Diffuser," AIAA Paper 1993-2239, June 1993.

[7] Zha, G. C., Knight, D., and Smith, D., "Numerical Investigations of High Speed Civil Transport Inlet Unstart Transient at Angle of Attack," *Journal of Aircraft*, Vol. 35, No. 6, 1998, pp. 851–856.

[8] Zha, G. C., Knight, D., and Smith, D., "Numerical Simulation of High Speed Civil Transport Inlet Operability with Angle of Attack," *AIAA Journal*, Vol. 36, No. 7, 1998, pp. 1223–1229.

[9] Cox, C., Lewis, C., and Pap, R.. "Prediction of Unstart Phenomena in Hypersonic Aircraft," AIAA Paper 1995-6018, April 1995.

[10] Schmitz, D. M., and Bissinger, N. C., "Design and Testing of Fixed-Geometry Hypersonic Intakes," AIAA Paper 1998-1529, April 1998.

[11] Van Wie, D. M., and Kwok, F. T., "Starting Characteristics of Supersonic Inlets," AIAA Paper 1996-2914, July 1996.

[12] Reinartz, B. U., and Herrmann, C. D., "Aerodynamic Performance Analysis of a Hypersonic Inlet Isolator Using Computation and

Experiment," *Journal of Propulsion and Power*, Vol. 19, No. 5, 2003, pp. 868–875.
[13] Emami, S., and Trexler, C. A., "Experimental Investigation of Inlet-Combustor Isolators for a Dual-Mode Scramjet at a Mach Number of 4," NASA TP 3502, May 1995.
[14] Hawkins, W. R., and Marquart, E. J.. "Two-Dimensional Generic Inlet Unstart Detection at Mach 2.5–5.0," AIAA Paper 1995-6019, April 1995.
[15] Voland, R. T., and Auslender, A. H., "CIAM/NASA Mach 6.5 Scramjet Flight and Ground Test," AIAA Paper 1999-4848, Nov. 1999.
[16] Kulkarni, S. R., Lugosi, G., and Venkatesh, S. S.. "Learning Pattern Classification-A Survey," *IEEE Transactions on Information Theory*, Vol. 44, No. 6, 1998, pp. 2178–2206.
[17] Liu, H., Yu, L., Dash, M., and Motoda, H., "Active Feature Selection Using Classes," *Pacific-Asia Conference on Knowledge Discovery and Data Mining*, Springer–Verlag Berlin, Heidelberg, 2003, pp. 474–485.
[18] Dash, M., and Liu, H., "Feature Selection for Classification," *Intelligent Data Analysis*, Vol. 1, No. 3, 1997, pp. 131–156.
[19] Kohavi, R., and John, G., "Wrappers for Feature Subset Selection," *Artificial Intelligence*, Vol. 97, No. 1–2, 1997, pp. 273–324.
[20] Guyon, I., and Elisseeff, A., "An Introduction to Variable and Feature Selection," *Journal of Machine Learning Research*, Vol. 3, No. 7–8, 2003, pp. 1157–1182.
[21] Hu, Q., Yu, D., and Xie, Z., "Information-Preserving Hybrid Data Reduction Based on Fuzzy-Rough Techniques," *Pattern Recognition Letters*, Vol. 27, No. 5, 2006, pp. 414–423.
[22] Guyon, I., Matic, N., and Vapnik, V.. "Discovering Informative Patterns and Data Cleaning," *Advances in Knowledge Discovery and Data Mining*, MIT Press, Cambridge, MA, 1996, pp. 181–203.
[23] Guyon, I., Weston, J., Barnhill, S., and Vapnik, V.. "Gene Selection for Cancer Classification Using Support Vector Machines," *Machine Learning*, Vol. 46, No. 1–3, 2002, pp. 389–422.
[24] Rakotomamonjy, A.. "Variable Selection Using SVM-Based Criteria," *Journal of Machine Learning Research*, Vol. 3, No. 7–8, 2003, pp. 1357–1370.
[25] Li, G., Yang, J., Liu, G., and Li, X., "Feature Selection for Multi-Class Problems Using Support Vector Machines," *Proceedings of the 8th Pacific Rim International Conference on Artificial Intelligence*, IEEE, Piscataway, NJ, Aug. 2004, pp. 292–300.
[26] Duan, K., Rajapakse, J. C., Wang, H., and Azuaje, F., "Multiple SVM-RFE for Gene Selection in Cancer Classification with Expression Data," *IEEE Transactions on Nanobioscience*, Vol. 4, No. 3, 2005, pp. 228–234.
[27] Yao, K., Lu, W., Zhang, S., Xiao, H., and Li, Y., "Feature Expansion and Feature Selection for General Pattern Recognition Problems," *IEEE International Conference on Neural Networks and Signal Processing*, IEEE Publications, Piscataway, NJ, Dec. 2003, pp. 29–32.
[28] Fisher, R. A., "The Use of Multiple Measurments in Taxonomic Problems," *Annual Eugenics*, Vol. 7, Part 2, 1936, pp. 179–188.
[29] Cui, Y., Swets, D., and Weng, J., "Learning-Based Hand Sign Recognition Using SHOSLIF-M," *Proceedings of the 5th International Conference on Computer Vision*, IEEE, Piscataway, NJ, 1995, pp. 631–636.
[30] Liu, K., Cheng, Y., Yang, J., Liu, L., and Liu, Y., "Discriminant Performance of the Algebraic Features of Handwritten Character Images," *Proceedings of the 12th IAPR International Conference on Pattern Recognition*, IEEE, Piscataway, NJ, 1994, pp. 426–428.
[31] Belhumeur, P. N., Hespanha, J. P., and Kriegman, D. J., "Eigenfaces vs. Fisherfaces: Recognition Using Class Specific Linear Projection," *IEEE Transactions on Pattern Analysis and Machine Intelligence*, Vol. 19, No. 7, 1997, pp. 711–720.

R. Bowersox
Associate Editor